MNRAS **460,** 2351–2359 (2016)
Advance Access publication 2016 May 13
doi:10.1093/mnras/stw1146

A spectroscopic study of the globular Cluster NGC 4147

S. Villanova,[1⋆] L. Monaco,[2⋆] C. Moni Bidin[3⋆] and P. Assmann[4,1]

[1]*Departamento de Astronomia, Universidad de Concepción, Casilla 160, Chile*
[2]*Departamento de Ciencias Fisicas, Universidad Andres Bello, Republica 220, Santiago, Chile*
[3]*Instituto de Astronomia, Universidad Catolica del Norte, Av. Angamos 0610, Antofagasta, Chile*
[4]*NAOC, Chinese Academy of Sciences, 20A Datun Rd, Chaoyang District, 100012 Beijing, China*

Accepted 2016 May 10. Received 2016 May 10; in original form 2016 February 1

ABSTRACT

We present the abundance analysis for a sample of 18 red giant branch stars in the metal-poor globular cluster NGC 4147 based on medium- and high-resolution spectra. This is the first extensive spectroscopic study of this cluster. We derive abundances of C, N, O, Na, Mg, Al, Si, Ca, Ti, Cr, Fe, Ni, Y, Ba, and Eu. We find a metallicity of [Fe/H] $= -1.84 \pm 0.02$ and an α-enhancement of $+0.38 \pm 0.05$ (errors on the mean), typical of halo globular clusters in this metallicity regime. A significant spread is observed in the abundances of light elements C, N, O, Na, and Al. In particular, we found an Na–O anticorrelation and Na–Al correlation. The cluster contains only ∼15 per cent of stars that belong to the first generation (Na-poor and O-rich). This implies that it suffered a severe mass-loss during its lifetime. Its [Ca/Fe] and [Ti/Fe] mean values agree better with the Galactic halo trend than with the trend of extragalactic environments at the cluster metallicity. This possibly suggests that NGC 4147 is a genuine Galactic object at odd with what claimed by some author that proposed the cluster to be member of the Sagittarius dwarf galaxy. An antirelation between the light *s*-process element Y and Na may also be present.

Key words: stars: abundances – globular clusters: individual: NGC4147.

1 INTRODUCTION

Galactic globular clusters (GGCs) are known to host star-to-star variations as far as chemical abundances are concerned. More specifically, Carretta et al. (2009b) showed that all GGCs studied up to now have at least a spread (or anticorrelation) in the content of their light-elements O and Na. The only confirmed exception is Ruprecht 106, where Villanova et al. (2013) found that stars share a homogenous chemical composition. This spread is probably due to the early evolution of each cluster, when a second generation of stars (Na-rich and O-poor) was born from gas polluted by ejecta of evolved stars of the first generation (Na-poor and O-rich). This is the so called multiple-population phenomenon.

Carretta et al. (2009b) showed also that most of the stars currently found in a globular cluster (GC) belong to the second generation (∼60/80 per cent). This is at odds with theory, which says that first-generation stars must have been much more numerous than what we observe nowadays in order to produce enough ejecta to form the second (D'Ercole et al. 2008). This contradiction can be partially explained if we assume that ejecta were collected preferentially in the centre of the cluster due to the gravitational potential. Because of this, the second generation was formed in the centre and was much less affected by the violent relaxation and the gas expulsion phase during the protocluster period (Khalaj & Baumgardt 2015) or by Galactic tidal disruption than the first, which lost most of its members (Caloi & D'Antona 2011).

On the other hand, Caloi & D'Antona (2011) suggested the possibility of the existence of clusters that retained almost all the first generation and so only a small fraction of the stars would belong to the second. An example of such a cluster is Terzan 8, where Carretta et al. (2014) found that almost all stars belong to the first generation.

Here we present an opposite case, the GC NGC 4147. This object has a horizontal branch (HB) that is mainly populated in the blue part. However, it shows also the presence of a red tail. According to Caloi & D'Antona (2011), this indicates that almost all its stars should belong to the second generation, with a fraction of first-generation objects that should be very small, probably smaller than all the other GGCs studied up to now. In order to verify this statement, we obtained spectroscopic data in the red giant branch (RGB) region with the aim of measuring their light-element content. We take advantage of these data also to perform a full chemical analysis of the cluster both to study the chemical trend of its multiple-populations and to compare it with different environments. This is because NGC 4147, based on the projection on the sky of the theoretical orbit of the Sagittarius dwarf spheroidal galaxy

⋆ E-mail: svillanova@astro-udec.cl. (SV); lmonaco1976@gmail.com (LM); chr.moni.bidin@gmail.com (CMB)

computed by Ibata & Lewis (1998), was suggested to be a possible former member of the galaxy (Bellazzini, Ferraro & Ibata 2003a), like NGC 5053 and NGC 5634, recently studied by Sbordone et al. (2015). Bellazzini et al. (2003b) also found evidence for the presence of Sgr tidal stream stars in the background of NGC 4147 using 2MASS data.

Law & Majewski (2010), on the other hand, used the spatial and kinematic data available for stars associated with the Sgr tidal stream to construct numerical model of the tidal disruption of the galaxy. These authors considered the association of NGC 4147 to Sgr as still possible, but with a low statistical confidence.

In Section 2, we describe data reduction and in Section 3 the methodology we used to obtain the chemical abundances. In Section 4, we present our results including a comparison with different environments (Galactic and extragalactic). Finally in Section 5, we give a summary of our findings.

2 OBSERVATIONS, DATA REDUCTION, AND ABUNDANCE ANALYSIS

Our data set consists of medium- and high-resolution spectra collected at the GIRAFFE (mounted at the VLT-UT2 telescope) and MIKE (mounted at the Magellan-Clay telescope) spectrograph, respectively.[1] Targets were selected from the Stetson, Catelan & Smith (2005) photometry. Three targets were in common between the two data sets.

We observed with GIRAFFE, a total of 17 RGB stars with magnitude between $V = 15.6$ and 18.0. We used the set-up HR12, that gives a spectral coverage between 5820 and 6140 Å with a resolution of $R = 18\,700$. The signal-to-noise (S/N) is between 25 and 70 at 6000 Å. Data were reduced using the dedicated pipeline (see http://www.eso.org/sci/software/pipelines/). Data reduction includes bias subtraction, flat-field correction, wavelength calibration, sky subtraction, and spectral rectification.

MIKE was used to observe six RGB stars with V magnitude between 14.7 and 15.6. The spectrograph cover a wide spectral range, from the ultraviolet to the near-infrared, with a resolution of $R = 32\,000$ (using a slit of 0.7 arcsec). The S/N of the spectra is between 70 and 90 at 6000 Å. Data were reduced using IRAF,[2] including bias subtraction, flat-field correction, wavelength calibration, scattered-light and sky subtraction, and spectral rectification.

Radial velocities were measured by the FXCOR package in IRAF, using a synthetic spectrum as a template. Stars with very different radial velocity with respect to the median value were rejected as non-member. We rejected also two GIRAFFE targets with a radial velocity similar to that of the cluster but with higher metallicities ([Fe/H] ~ -1.60). These two stars have low S/N and we could use only one out of the three iron lines available to measure [Fe/H] (see next section). So the disagreement in metallicity is probably due to the combination of the two factors. We end up with a sample of 12 GIRAFFE and 6 MIKE targets. The mean radial velocity we obtained is 179.9 ± 0.5 km s^{-1}. Peterson, Olszewski & Aaronson (1986) and Pryor et al. (1988) give 183.5 ± 1.3 and 183.2 ± 0.9 instead. However the first is based on one star only, while the second does not give any detail on the radial velocity measurements they perform so we cannot suggest any reason for this discrepancy. If we compare the mean radial velocity obtained with the two instruments, we get 179.4 ± 0.5 for GIRAFFE, and 180.7 ± 1.0 for MIKE (errors on the mean). The two values well agree within 1σ. Table 1 lists the basic parameters of the retained stars: ID (from Stetson et al. 2005), J2000.0 coordinates (RA & Dec. in degrees), B and V magnitudes, heliocentric radial velocity RV_H (km s^{-1}), T_{eff} (K), log(g), microturbulence velocity v_t (km s^{-1}), plus [Fe/H], [Na/Fe], [Ca/Fe], and [Ba/Fe] abundances. The determination of the atmospheric parameters and abundances is discussed in the next section. In Fig. 1 we report, on the top of the cluster colour–magnitude diagram (CMD), the MIKE targets as black filled squares, and with open black circles the GIRAFFE targets.

3 ABUNDANCE ANALYSIS

Atmospheric parameters were obtained in the following way. First, T_{eff} was derived from the $B - V$ colour using the relation of Ramirez & Melendez (2005). The reddening we adopted ($E(B - V) = 0.02$) was obtained from Harris (1996, 2010 edition). Surface gravities (log(g)) were obtained from the canonical equation:

$$\log\left(\frac{g}{g_\odot}\right) = \log\left(\frac{M}{M_\odot}\right) + 4\log\left(\frac{T_{eff}}{T_\odot}\right) - \log\left(\frac{L}{L_\odot}\right),$$

where the mass $M/M_\odot$ was assumed to be $0.8\,M_\odot$, and the luminosity $L/L_\odot$ was obtained from the absolute magnitude M_V assuming an apparent distance modulus of $(m–M)_V = 16.49$ (Harris 1996). The bolometric correction (BC) was derived by adopting the relation BC–T_{eff} from Alonso, Arribas & Martinez-Roger (1999). Finally, microturbulence velocity (v_t) was obtained from the relation of Marino et al. (2008).

Atmospheric models were calculated using ATLAS9 (Kurucz 1970) assuming our estimations of T_{eff}, log(g), and v_t, and the [Fe/H] value from Harris (1996)([Fe/H] $= -1.80$).

The local thermodynamic equilibrium (LTE) programme MOOG (Sneden 1973) was used for the abundance analysis. For MIKE data, T_{eff}, log(g), and v_t were re-adjusted and new atmospheric models calculated in an interactive way in order to remove trends in excitation potential and equivalent width versus abundance for T_{eff} and v_t, respectively, and to satisfy the ionization equilibrium for log(g). 30/40 Fe I and 8/10 Fe II (depending on the S/N of the spectrum) were used for the latter purpose. The [Fe/H] value of the model was changed at each iteration according to the output of the abundance analysis.

For GIRAFFE data, we measured Fe, Na, Ca and Ba abundances. Fe abundances were obtained from the equivalent width of the three iron lines at 5914, 5930, and 6065 Å, while for Na we compared the strength of the NaD doublet at 589 nm with suitable synthetic spectra calculated for five different abundances. Finally Ca and Ba abundances were obtained from the lines at 5857, 6102, and 5853, respectively, using spectrosynthesis. MIKE data allowed us to perform a more complete abundance analysis and we present here our measurements for C, N, O, Na, Mg, Al, Si, Ti, Cr, Fe, Ni, Y, Ba, and Eu. The line-list and the methodology we used are the same used in previous papers (e.g. Villanova et al. 2013), so we refer to those articles for a detailed discussion about this point. Here, we just underline that we took hyperfine splitting into account for Ba. Na abundances were corrected for NLTE using the corrections provided

[1] Observations were taken with ESO telescopes at the La Silla-Paranal Observatory under programme ID 083.D-0530, and with LCO telescopes at the Magellan observatory under programme ID CN2011B-039.

[2] IRAF is distributed by the National Optical Astronomy Observatory, which is operated by the Association of Universities for Research in Astronomy, Inc., under cooperative agreement with the National Science Foundation.

Table 1. Parameters for the observed stars including Fe I, Na I, Ca I and Ba II abundances. Reported errors are errors on the mean.

ID	RA	Dec.	B	V	RV_H	T_{eff}	log(g)	v_t	[Fe/H]	[Na/Fe]	$[Na/Fe]_{NLTE}$	[Ca/Fe]	[Ba/Fe]
						GIRAFFE							
D1	182.559 08	18.533 58	17.641	16.845	180.2	4910	2.17	1.38	− 1.77	0.48	0.47	0.28	− 0.22
D8	182.531 50	18.518 26	16.128	15.086	178.0	4480	1.23	1.62	− 1.81	0.39	0.52	0.44	− 0.23
S268	182.506 58	18.526 11	17.355	16.542	180.3	4840	2.02	1.42	− 1.80	0.47	0.48	0.25	− 0.41
S377	182.470 29	18.558 02	17.506	16.725	177.9	4880	2.11	1.39	− 1.86	0.73	0.73	0.55	− 0.04
S408	182.503 79	18.554 02	17.496	16.701	177.3	4880	2.10	1.40	− 1.81	0.54	0.54	0.29	− 0.31
S414	182.508 37	18.534 66	17.642	16.849	180.2	4910	2.18	1.38	− 1.80	0.56	0.55	0.51	− 0.34
S429	182.514 87	18.539 25	16.830	15.950	178.7	4710	1.71	1.49	− 1.90	0.70	0.75	0.59	–
S432	182.515 87	18.563 22	16.756	15.777	178.7	4670	1.62	1.52	− 1.86	0.60	0.67	0.52	− 0.20
S445	182.519 76	18.552 26	16.267	15.296	181.0	4540	1.35	1.59	− 1.75	0.39	0.50	0.30	− 0.23
S688	182.531 12	18.534 97	16.619	15.688	182.1	4640	1.57	1.53	− 1.82	0.49	0.57	0.34	0.03
S690	182.534 59	18.535 44	16.556	15.629	177.6	4630	1.54	1.54	− 1.71	0.51	0.59	0.33	− 0.31
S692	182.535 87	18.548 86	17.532	16.737	181.3	4880	2.12	1.39	− 1.92	0.61	0.61	0.58	− 0.12
Cluster									− 1.79	0.48	0.58	0.42	− 0.22
error									0.03	0.05	0.03	0.04	0.04
						MIKE							
D8	182.531 50	18.518 26	16.128	15.086	178.9	4430	0.80	1.70	− 1.84	0.56	0.46	0.38	− 0.19
S437	182.516 97	18.548 16	15.885	14.716	184.0	4300	0.45	1.80	− 1.88	− 0.03	− 0.11	0.39	− 0.22
S445	182.519 76	18.552 26	16.267	15.296	181.9	4460	0.75	1.59	− 1.86	0.69	0.59	0.35	− 0.17
S454	182.522 53	18.543 05	16.257	15.266	177.8	4470	0.85	1.67	− 1.84	0.47	0.36	0.45	− 0.15
S468	182.525 24	18.546 25	15.791	14.702	182.6	4300	0.22	1.79	− 1.91	0.18	0.10	0.37	− 0.04
S690	182.534 59	18.535 44	16.556	15.629	179.2	4570	1.14	1.53	− 1.82	0.71	0.57	–	− 0.05
Cluster									− 1.86	0.43	0.33	0.39	− 0.14
error									0.01	0.12	0.11	0.02	0.03
Δ(GIR-MIK)	–	–	–	–	–	+63	+0.48	− 0.03	+0.08	–	–	+0.00	− 0.12

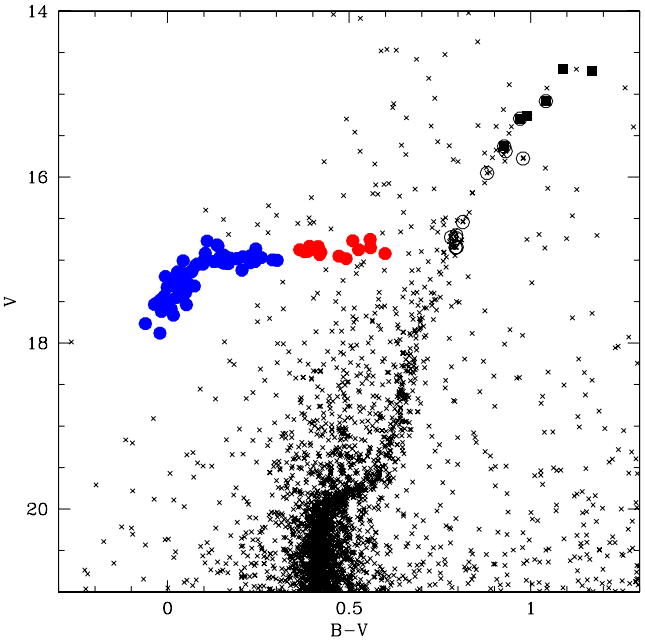

Figure 1. V versus $B - V$ CMD of NGC 4147. Open black circles indicate GIRAFFE targets, while filled black circles indicate MIKE targets. HB stars were divided in first-generation (filled red circles) and second-generation (filled blue circles) objects. See the text for more details.

by the INSPEC [3] data base. After the NLTE correction, we found a small offset of 0.24 dex between Na abundances of the two data sets, that we could estimate using the three stars in common (#S445, #S690, #D8). This is very likely due to some systematic error in the abundance determination of the NaD doublet. This feature is saturated and then its abundance very sensitive to any error in the flat-field or continuum normalization. In order to remove it, we applied a correction of +0.24 dex to GIRAFFE NaD measurements. Abundances for each target are reported in Tables 1 and 2, together with the mean values and the error on the mean.

A detailed internal error analysis was performed by varying T_{eff}, log(g), [Fe/H], and v_t and redetermining abundances of star #D8, assumed to represent the entire MIKE sample. GIRAFFE data will not be used to check for intrinsic spreads, so error analysis is not required for them. We just give in Table 1 the mean differences in T_{eff}, log(g), v_t, [Fe/H], [Ca/Fe], and [Ba/Fe] with respect MIKE data based on the three stars in common. Parameters for stars #D8 were varied by $\Delta T_{eff} = +50$ K, $\Delta \log(g) = +0.10$, Δ[Fe/H] $= +0.05$ dex, and $\Delta v_t = +0.05$ km s^{-1}. This estimation of the internal errors for atmospheric parameters was performed as in Marino et al. (2008). Results are shown in Table 3, including the error due to the noise of the spectra. This error was obtained for elements whose abundance was obtained by EQWs, as the errors on the mean given by MOOG, and for elements whose abundance was obtained by spectrum-synthesis, as the error given by the fitting procedure. σ_{tot} is the squared sum of the single errors, while σ_{obs} is the mean observed dispersion of MIKE data.

As a cross check of our abundance analysis, we plot in Figs 2 and 3 [Fe/H], [Na/Fe], [Ca/Fe], and [Ba/Fe] versus T_{eff} for the entire sample. The temperature range covered by our stars is about 600 K. As far as iron, calcium and barium are concerned, a linear fit gives a slopes with a significance below 1σ. We plot also the mean abundance for each element and the $\pm$ 1σ error. Again all stars are spread around the mean value and no sign of trend is present. After this check, we conclude that the two different methods we used for GIRAFFE and MIKE targets are consistent over the entire temperature range.

[3] Version 1.0 (Karin Lind et al.; http://inspect.coolstars19.com/index.php?n = Main.HomePage).

Table 2. Chemical abundances of MIKE stars. The abundance for Ti is the mean of those obtained from the neutral and singly ionized species. Reported errors are errors on the mean.

ID	(CI/Fe)	(NI/Fe)	(OI/Fe)	(CNO/Fe)	(MgI/Fe)	(AlI/Fe)	(SiI/Fe)	(Ti/Fe)	(CrI/Fe)	(NiI/Fe)	(YII/Fe)	(EuII/Fe)
D8	− 0.72	0.86	− 0.13	0.07	0.38	0.95	0.44	0.30	− 0.16	0.03	− 0.22	0.45
S437	− 0.24	0.21	0.30	0.21	0.47	0.25	0.47	0.31	− 0.11	− 0.06	− 0.01	0.38
S445	− 0.64	0.75	− 0.27	− 0.04	0.38	1.03	0.44	0.25	− 0.18	− 0.08	− 0.33	0.33
S454	− 0.26	0.60	0.17	0.17	0.50	0.91	–	0.33	− 0.23	− 0.07	− 0.35	0.37
S468	− 0.53	0.54	0.26	0.20	0.46	0.27	0.49	0.27	− 0.14	− 0.07	− 0.11	0.27
S690	− 0.61	0.80	0.06	0.14	0.34	1.01	–	0.25	–	− 0.05	− 0.43	0.42
Cluster	− 0.50	0.63	0.07	0.12	0.42	0.74	0.46	0.28	− 0.16	− 0.05	− 0.24	0.37
error	0.08	0.10	0.09	0.04	0.03	0.15	0.01	0.01	0.02	0.02	0.06	0.03

Table 3. Estimated errors on abundances due to errors on atmospheric parameters and to spectral noise compared with the observed errors for stars #D8. The last column gives the observed dispersion of MIKE data.

ID	$\Delta T_{\rm eff} = 50$ K	$\Delta\log(g) = 0.10$	$\Delta v_{\rm t} = 0.05$ km s^{-1}	Δ[Fe/H] = 0.05	S/N	$\sigma_{\rm tot}$	$\sigma_{\rm obs}$
Δ([C/Fe])	0.02	0.02	0.05	0.04	0.02	0.07	0.20 ± 0.06
Δ([N/Fe])	0.05	0.02	0.05	0.03	0.02	0.08	0.23 ± 0.07
Δ([O/Fe])	0.05	0.06	0.05	0.02	0.02	0.10	0.23 ± 0.07
Δ([Na/Fe])	0.02	0.01	0.00	0.01	0.05	0.06	0.30 ± 0.09
Δ([Mg/Fe])	0.03	0.01	0.00	0.01	0.05	0.06	0.06 ± 0.02
Δ([Al/Fe])	0.02	0.00	0.02	0.01	0.05	0.06	0.39 ± 0.11
Δ([Si/Fe])	0.05	0.01	0.02	0.01	0.05	0.07	0.02 ± 0.01
Δ([Ca/Fe])	0.00	0.00	0.00	0.00	0.04	0.04	0.04 ± 0.01
Δ([Ti/Fe])	0.03	0.00	0.00	0.01	0.03	0.04	0.03 ± 0.01
Δ([Cr/Fe])	0.03	0.00	0.00	0.00	0.03	0.04	0.05 ± 0.01
Δ([Fe/H])	0.05	0.01	0.02	0.01	0.01	0.05	0.03 ± 0.01
Δ([Ni/Fe])	0.00	0.00	0.00	0.00	0.02	0.02	0.04 ± 0.01
Δ([Y/Fe])	0.07	0.04	0.03	0.00	0.04	0.09	0.16 ± 0.05
Δ([Ba/Fe])	0.03	0.05	0.03	0.03	0.01	0.07	0.07 ± 0.02
Δ([Eu/Fe])	0.05	0.03	0.03	0.02	0.02	0.07	0.04 ± 0.01

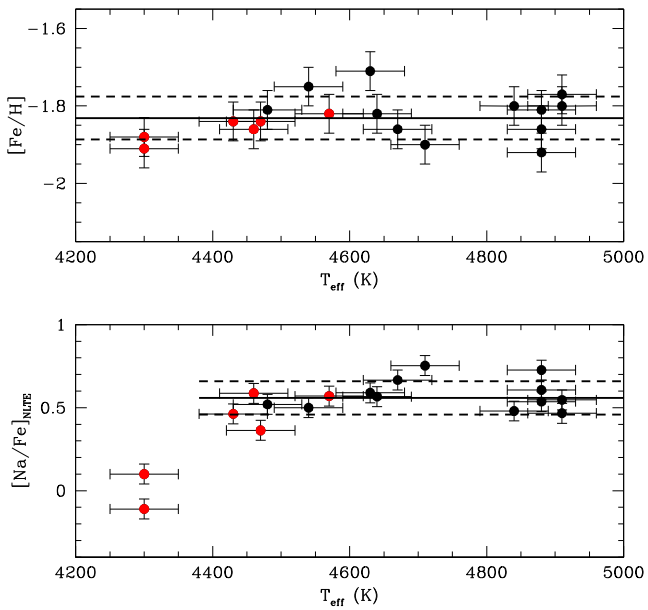

Figure 2. [Fe/H] versus $T_{\rm eff}$ (upper panel) and [Na/Fe] versus $T_{\rm eff}$ (lower panel) relations for our sample. GIRAFFE targets are reported as black circles, while MIKE targets are reported as red circles. Error adopted are those from Table 3. For both relations, we indicated the mean value with a continuous black line and the ± 1σ interval with two dashed lines. For the [Na/Fe] versus $T_{\rm eff}$ relation, we considered only targets hotter than 4400 K. See the text for more details.

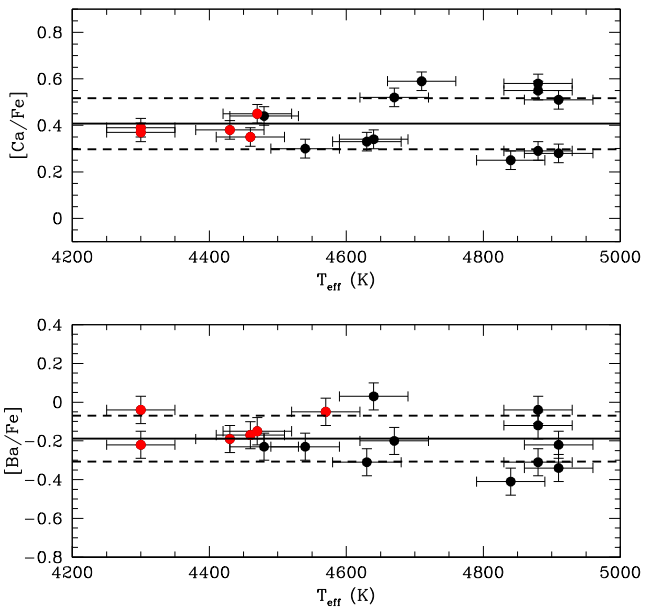

Figure 3. [Ca/Fe] versus $T_{\rm eff}$ (upper panel) and [Ba/Fe] versus $T_{\rm eff}$ (lower panel) relations for our sample. GIRAFFE targets are reported as black circles, while MIKE targets are reported as red circles. Error adopted are those from Table 3. For both relations, we indicated the mean value with a continuous black line and the ± 1σ interval with two dashed lines.

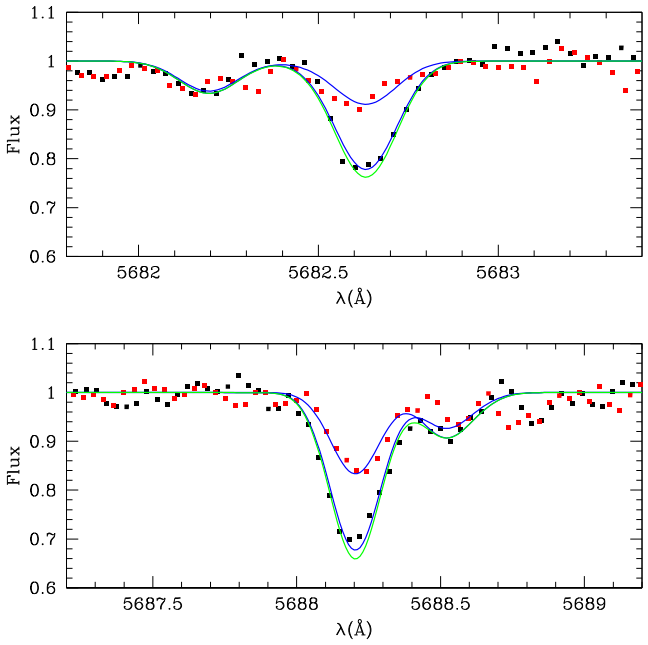

Figure 4. Spectra of the #D8 (black squares) and #S437 (red squares) targets around the Na double at 568 nm. Blue lines are the best-fitting synthetic spectra with Na abundances taken from Table 1. The green line is a synthetic spectrum calculated for the atmospheric parameters of #S437 but with the Na content of #D8.

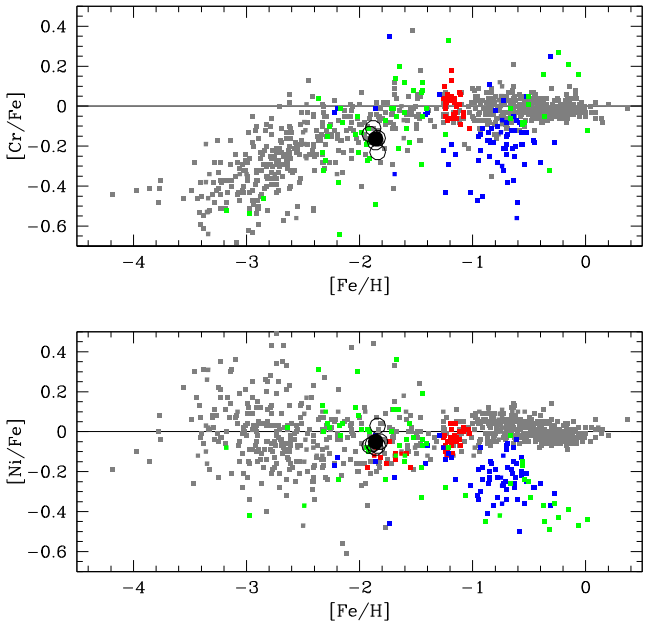

Figure 5. [Cr/Fe] and [Ni/Fe] trends as a function of [Fe/H] for different environments (see the text). Open black circles indicate MIKE targets, while the filled black circle is the mean abundance of NGC 4147.

If we move to Na instead, we see a different situation. First of all, we considered only stars with temperature hotter than 4400 K. Again a linear fit gives a slopes with a significance below 1σ and all stars are spread around the mean value with no sign of any trend. However, the two coldest targets show an Na content much lower than that of their hotter companions. If we extrapolate the fit to the temperature of the two coldest stars, we find a difference with respect to the fit of $\sim$0.50 dex, that is significant at a level of $\sim 4\sigma$. This is because they are first-generation stars with an intrinsic low Na, while all the other targets are second-generation stars with high Na. In order to show visually the large difference in Na content of the two coldest stars with respect to the rest of the sample we plot in Fig. 4, the spectra of the Na-rich #D8 (black squares) and the Na-poor #S437 (red squares) target around the Na double at 568 nm. Blue lines are the best-fitting synthetic spectra with Na abundances taken from Table 1. The green line is a synthetic spectrum calculated for the atmospheric parameters of #S437 but with the Na content of #D8. It is clear from this comparison that the #S437 strong Na under abundance is real and not due, for instance, to the low S/N or to an ill-estimated stellar effective temperature.

4 RESULTS

4.1 Iron-peak elements

The iron content we obtained from GIRAFFE data is

$$[\mathrm{Fe/H}]_{\mathrm{GIRAFFE}} = -1.82 \pm 0.02$$

while from MIKE data is

$$[\mathrm{Fe/H}]_{\mathrm{MIKE}} = -1.86 \pm 0.01.$$

Reported errors are errors on the mean. The difference between the two data sets is of 0.04 dex, that correspond to 1.8σ. The agreement is satisfactory. Finally, we can give a value for the iron content of the cluster that is the mean of the two data sets:

$$[\mathrm{Fe/H}] = -1.84 \pm 0.02.$$

This value well agrees with Ivans (2009), that give [Fe/H] $= -1.7 \pm 0.1$, and with Harris (1996) that give [Fe/H] $= -1.80$. The measured iron dispersion in Table 3 well agrees with the dispersion due to measurement errors so we can rule out any intrinsic Fe abundance spread.

The chemical abundances for the iron-peak elements Cr and Ni are listed in Table 2. The value is subsolar for Cr, while Ni is basically solar-scaled. Fig. 5 (as well as the following plots) shows the mean (black filled circle) and star by star (black empty circles) elemental abundances of the cluster compared with a variety of galactic and extragalactic objects. We have included values from GGCs (Carretta et al. 2009b; Villanova, Geisler & Piotto 2010; Villanova & Geisler 2011, red filled squares); Disc and halo stars (Fulbright 2000; Reddy et al. 2003; Cayrel et al. 2004; Simmerer 2004; Barklem et al. 2005; Reddy, Lambert & Allende Prieto 2006; Francois et al. 2007, grey filled squares) and extragalactic objects such as Magellanic Clouds (Johnson, Ivans & Stetson 2006; Pompeia et al. 2008; Mucciarelli et al. 2008, 2009, blue filled squares), Draco, Sextans, Ursa Minor and Sagittarius dwarf galaxy and the ultrafaint dwarf spheroidals Boötes I and Hercules (Shetrone, Cote & Sargent 2001; Monaco et al. 2005; Sbordone et al. 2007; Koch et al. 2008; Ishigaki et al. 2014, green filled squares).

Around NGC 4147 metallicity, Galactic and extragalactic environments share the same iron-peak abundances, with only very few extragalactic stars showing a Cr depletion. NGC 4147 iron-peak elements agree with both environments and do not support or disproof an extragalactic origin of this object.

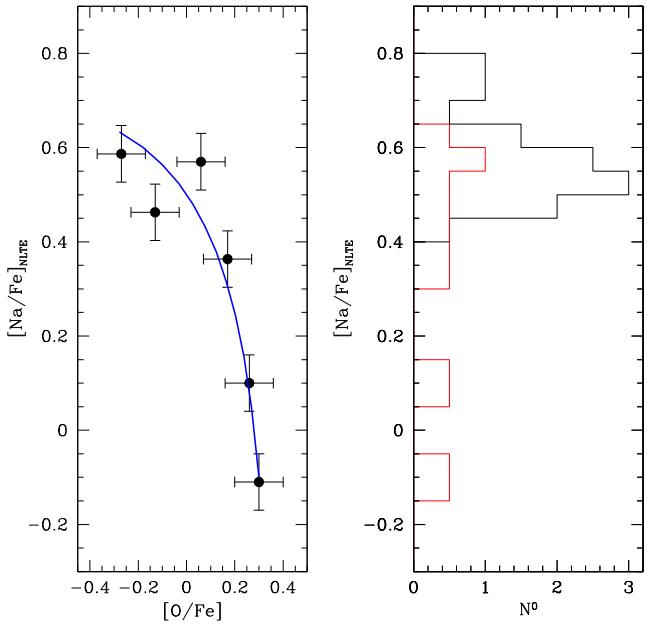

Figure 6. Left panel: [Na/Fe] versus [O/Fe] as obtained for MIKE targets. The cluster shows the typical Na-O anti-correlation of GGCs. The blue line is the Carretta et al. (2009a) dilution model for the cluster. Right panel: The Na distribution of GIRAFFE (black) and MIKE (red) targets. See the text for more details.

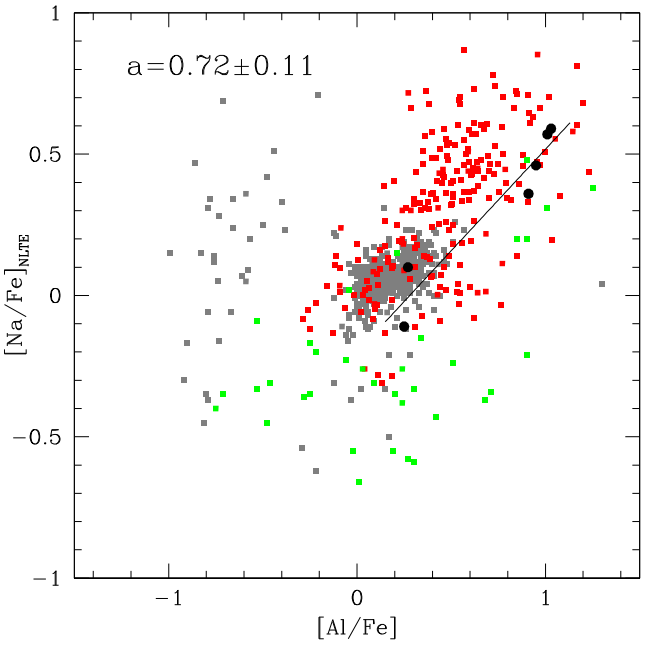

Figure 7. [Na/Fe] versus [Al/Fe] as obtained for MIKE targets (filled black circles). The cluster shows the typical Na-Al correlation of GGCs (red squares). See the text for more details.

4.2 Light elements

Light elements C, N, O, Na and Al have an observed spread that well exceeds the observational uncertainties (see Table 3). The only exception is Mg that seems to be homogeneous within the errors.

Very interesting is the analysis of the Na and O distributions. In Fig. 6, we show the Na–O anticorrelation of MIKE data on the left-hand panel, while in the right-hand panel we report the Na distribution based on the GIRAFFE and MIKE data. We fitted the Carretta et al. (2009a) dilution model (blue line) to the Na–O anticorrelation. According to this fit, the cluster is composed by a first generation of stars with [Na/Fe] $\sim +0.0$ and [O/Fe] $\sim +0.3$ and second generation with [Na/Fe] $\sim +0.5$ and [O/Fe] ~ -0.2. This is in common with all but one of the GCs studied up to now. The difference appears when we count the number of stars for each population. If we combine together the two data sets and consider all the stars with [Na/Fe]<0.30 as first generation, we end up with the result that that second-generation stars in the cluster represent $\sim$90 per cent of the total, leaving room only for a $\sim$10 per cent to the first generation. The Poissonian error related with the two estimations is 20 and 10 per cent, respectively. This result is confirmed by Fig. 1. Here, we selected tentatively the HB progeny of the first generation as red filled circles, and the HB progeny of the second generation as blue filled circles. If we compare the relative number of stars, we obtain that second-generation stars in the cluster represent 80 $\pm$ 10 per cent of the total. However, we point out that this number is a lower limits because we left out blue HB stars evolved off the blue HB zero age sequence, and at the same time red HB stars suffer a contamination from the field. So our best estimation is that $\sim$85 per cent of the stars in NGC 4147 belong to the second generation. If Caloi & D'Antona (2011) or Khalaj & Baumgardt (2015) are right, we have here a cluster that suffered an extreme loss of its first generation.

In Fig. 7, we show the correlation between Na and Al, another elements usually but not always involved in the light-element spread

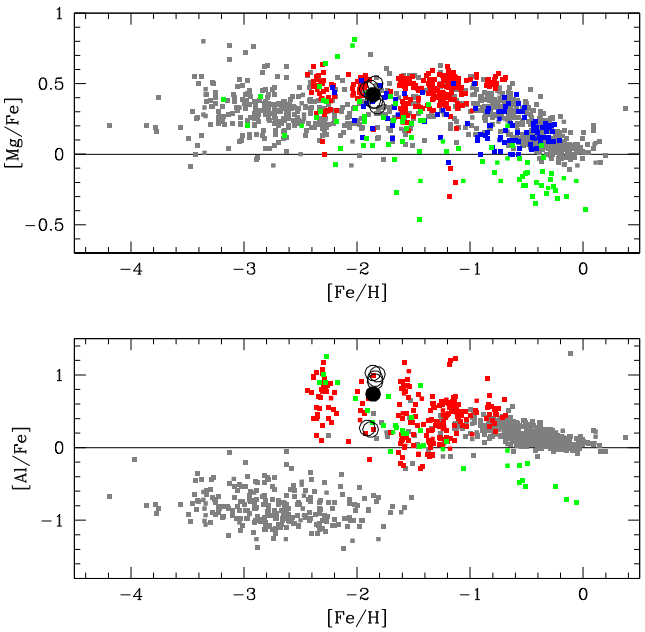

Figure 8. [Mg/Fe] and [Al/Fe] trends as a function of [Fe/H] for different environments (see the text). Open black circles indicate MIKE targets, while the filled black circle is the mean abundance of NGC 4147.

(Villanova & Geisler 2011). The cluster shows a clear correlation that matches that found in the other GGCs. In addition the two first-generation stars ([Na/Fe]$\sim$0.0, [Al/Fe]$\sim$0.2) well agrees with the bulk of Galactic objects while very few extragalactics targets occupy this region. In the figure, we report also the slope and its error. The significance of the relation of $\sim 7\sigma$.

Finally in Fig. 8, we show the Mg and Al versus Fe trends. NGC 4147 nicely follow the galactic and extragalactic trend as far as Mg is concern. Al shows a more surprising behaviour. If we consider only

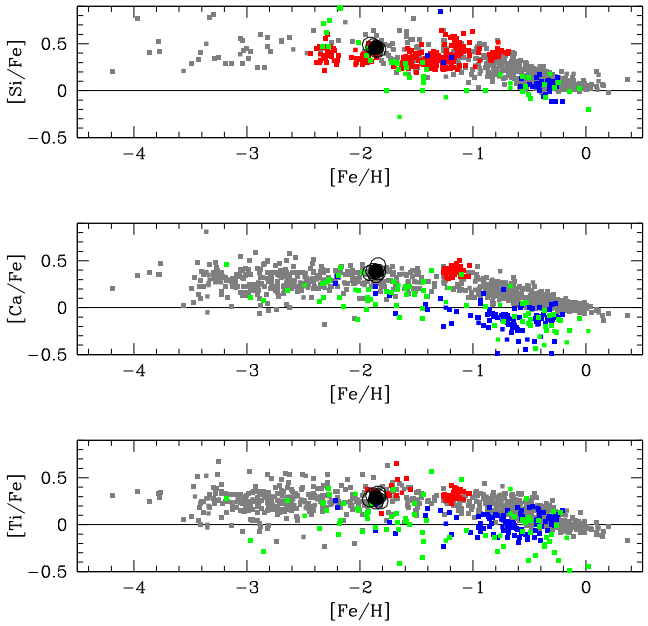

Figure 9. [Si/Fe], [Ca/Fe] and [Ti/Fe] trends as a function of [Fe/H] for different environments (see the text). Open black circles indicate MIKE targets, while the filled black circle is the mean abundance of NGC 4147.

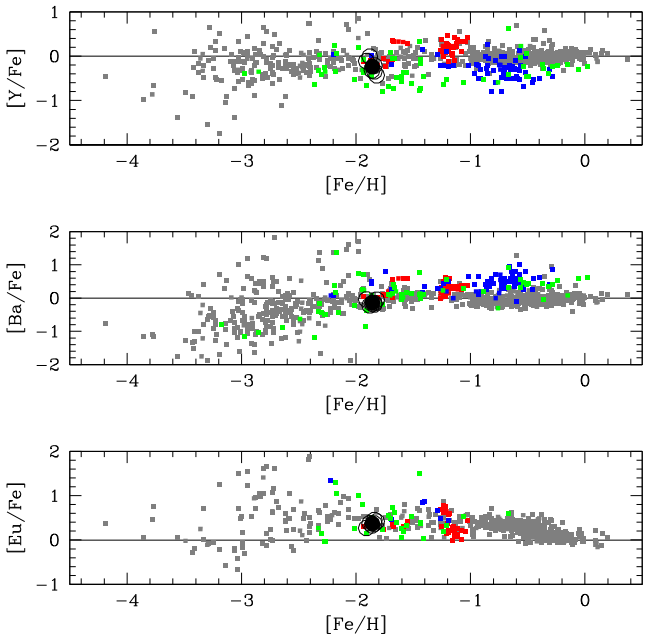

Figure 10. [Y/Fe], [Ba/Fe] and [Eu/Fe] trends as a function of [Fe/H] for different environments (see the text). Open black circles indicate MIKE targets, while the filled black circle is the mean abundance of NGC 4147.

Milky Way stars, they follow two separate trends. Almost all stars above [Fe/H] ~ -1.7 have [Al/Fe]$\geq$0, while all stars below [Fe/H] ~ -1.7 have [Al/Fe] well below 0 with a mean value of ~ -0.8. This result is not totally new, because Gehren et al. (2006, Fig. 5) found the same behaviour using [Al/Mg] versus [Fe/H] instead of [Al/Fe] versus [Fe/H] as we do. The surprise arises when we add GGC and extragalactic dwarfs because in both classes of objects stars below [Fe/H] ~ -1.7 have [Al/Fe]$\geq$0. This could suggest a different formation history of GCC stars with respect the halo field. In any case, NGC 4147 follow the GCC trend.

4.3 α elements

The α elements Si, Ca, and Ti are overabundant compared to the Sun. This is a common feature among almost every GGC as well as among similarly metal-poor field stars in the Milky Way and in outer galaxies. The calcium content we obtained from GIRAFFE data is

$$[\mathrm{Ca/Fe}]_{\mathrm{GIRAFFE}} = +0.42 \pm 0.04$$

while from MIKE data is

$$[\mathrm{Ca/Fe}]_{\mathrm{MIKE}} = +0.39 \pm 0.02.$$

Reported errors are errors on the mean. The difference between the two data sets is of 0.03 dex, within 1σ. The agreement is satisfactory. Based on Mg, Si, Ca, and Ti abundances of MIKE stars, we derive for the cluster a mean α element abundance of

$$[\alpha/\mathrm{Fe}] = +0.39 \pm 0.04$$

Fig. 9 shows the α-element abundance of the cluster (MIKE data only), compared with the trend as a function of the metallicity for GGCs, disc and halo stars and extragalactic objects. The α elements in NGC 4147 follows the same trend as GGCs and are fully compatible with halo field stars. Again NGC 4147 falls in a region where both Galactic and extragalactic objects overlap. However if we look carefully at the Ca trend, we notice that at the metallicity of the cluster the mean Ca abundance for halo stars is higher than that for dwarf galaxies. The difference is of $\sim$0.3 dex. This is true also for Ti. NGC 4147 stars have

$$[\mathrm{Ca/Fe}] = +0.40 \pm 0.02$$

and

$$[\mathrm{Ti/Fe}] = +0.28 \pm 0.02.$$

(reported errors are errors on the mean) that must be compared with the mean values for the halo ([Ca/Fe] $\sim$ 0.3, [Ti/Fe] $\sim$ 0.3) and for the Dwarf galaxies ([Ca/Fe] $\sim$ 0.1, [Ti/Fe] $\sim$ 0.1). So, according to its α-element content, NGC 4147 seems more likely to be a genuine Galactic cluster, although some other clusters like M54 and Arp2, that belong to the Sagittarius galaxy, have an α-element content similar to NGC 4147 ([Ca/Fe] = +0.32 and [Ca/Fe] = +0.46, respectively; Mottini, Wallerstein & McWilliam 2008; Carretta et al. 2010).

4.4 Heavy elements

While light-element variations are well known in GCs, intrinsic dispersion among heavier elements is less common. Most of the heavier elements ($Z > 30$) are produced either by slow or rapid neutron-capture reactions (the so-called *s* and *r* processes). *s*-process happens in a different physical condition with respect to *r*-process and are thus likely to happen in different astrophysical sites. We measured the abundances of the neutron-capture elements: Y, Ba, and Eu. Y and Ba are mainly produced by the *s*-process at solar metallicity, while Eu is produced almost exclusively in the *r*-process. The mean Y and Ba abundance ratios are slightly subsolar, while Eu is heavily supersolar. Fig. 10 shows the mean heavy-element ratios of the cluster (MIKE data only), compared with the trend as a function of the metallicity of GGCs, disc and halo stars and extragalactic objects. All three elements agree with Milky Way halo as well as with extragalactic environment. Fig. 11 shows the mean [Ba/Y] and

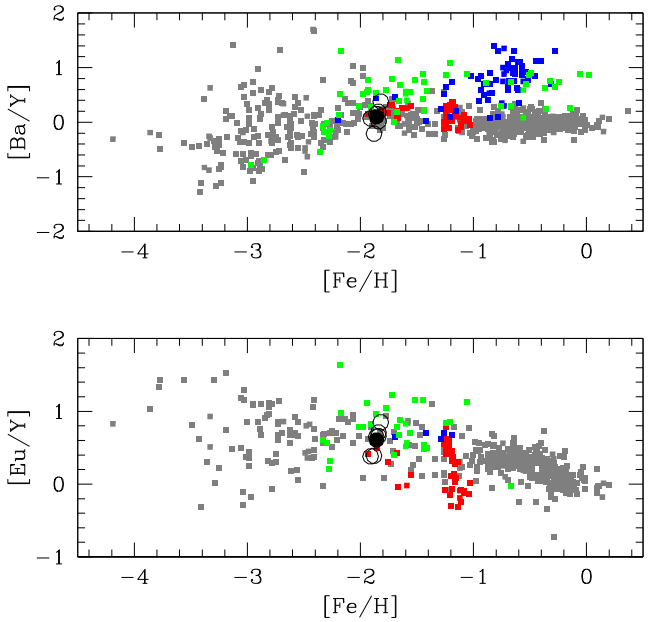

Figure 11. [Ba/Y] and [Eu/Y] trends as a function of [Fe/H] for different environments (see the text). Open black circles indicate MIKE targets, while the filled black circle is the mean abundance of NGC 4147.

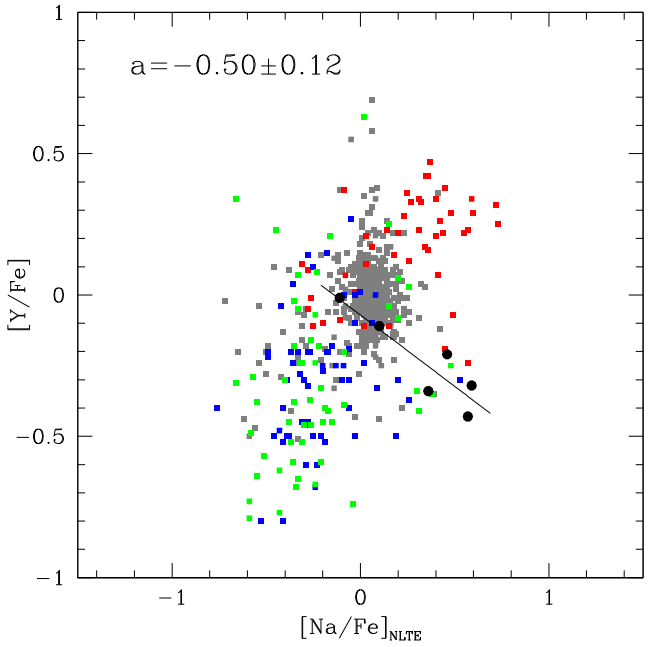

Figure 12. [Y/Fe] versus [Na/Fe] as obtained for MIKE targets (filled black circles). The cluster shows a possible Y–Na anticorrelation. See the text for more details.

[Eu/Y] ratios, where again NGC 4147 agrees both with the Galactic and the extragalactic trends

Ba and Eu show an observed spread that is comparable to that expected from the errors (see Table 3), while for Y the observed spread is significantly larger. To check this behaviour, we show in Fig. 12 the abundance ratios of [Y/Fe] as a function of [Na/Fe]. The two first-generation stars ([Na/Fe]∼0.0) well agrees with the bulk of Galactic objects while most of the extragalactic stars have lower Na and Y content. This support our identification of NGC 4147 as a Galactic cluster. What is more interesting is the anticorrelation between Y and Na with Y that decreases while Na increases. In the plot, we reported the slope a of the linear fit to NGC 4147 stars (black line) together with its error. The significance of the fit is larger than 4σ.

Only a handful of metal-poor GCs show a potential star-to-star dispersion in neutron-capture elements (Kacharov, Koch & McWilliam 2013; Worley et al. 2013). Marino et al. (2009) found a wide range of abundances values for *s*-process elements, Y, Zr and Ba, in M22. They also identified a bimodality among these elements. However, none of the elements show a correlation with Na, O and Al.

Our result implies that the second Na-rich generation was formed by material where Y was destroyed. This is at odd with current models that describe the multiple population phenomenon in GCs, which postulate AGB stars as major polluters (Ventura & D'Antona 2009). In fact, AGB stars also produce light *s*-process elements like Y (Cristallo et al. 2015). The amount of light *s*-element produced depends a lot on the mass of the AGB star, but in no case a Y destruction is predicted. For this reason, we checked for possible blending not considered in our line-list. For example, a blend with a CN or CH line could mimic a [Y/Fe] spread even if Y is constant just because C and N vary. However, the result of this check was negative. We underline also that the fact that the two Y-rich first-generation stars are also the two coldest objects in our sample. We have no first-generation stars in the temperature range of the second-generation targets, so we cannot totally rule out a possible temperature effect on our Y abundance determination. In spite of that, we leave open the possibility that the [Y/Fe] versus [Na/Fe] trend we found is real waiting for future studies.

5 SUMMARY

In this paper, we present the first detailed chemical abundances of 15 elements in six red giant radial velocity members of NGC 4147 observed using the high-resolution MIKE spectrograph, mounted at the Magellan-Clay telescope, and Fe and Na abundances in 12 red giant radial velocity members observed using the medium resolution GIRAFFE spectrograph, installed at the VLT-UT2 telescope. Chemical abundances have been computed using plane-parallel atmospheric-models and LTE approximation. Equivalent width method has been used when possible. Otherwise we applied the spectrum-synthesis method. We obtained the following results.

(i) We found a mean metallicity of [Fe/H] $= -1.84 \pm 0.02$, that well agree with previous literature data. As far as other iron-peak elements are concerned, Cr is subsolar while Ni is solar-scaled, in agreement with halo and dwarf galaxies environment at the cluster metallicity.

(ii) NGC 4147 shows the typical Na–O anticorrelation common to almost all the other GGCs. However, the cluster contains only ∼15 per cent of first-generation stars. This implies that it suffered a severe mass-loss, maybe the most extreme among all the GGCs. Na is also correlated with Al as found in many GGCs. Mg follows the Galactic trend, while Al is much more enhanced with respect to halo stars sharing this behaviours with all the other GGCs.

(iii) NGC 4147 has the typical α-enhancement of the halo. Its Ca and Ti abundances agree better with the halo than with the mean Ca and Ti content of extragalactic environments at the cluster metallicity. This is true also if we consider the behaviour of [Na/Fe] versus [Al/Fe] and [Y/Fe] versus [Na/Fe].

(iv) Heavy elements Y, Ba and Eu have mean abundances that match those of the Milky Way and of extragalactic environments.

While Ba and Eu are homogeneous, Y possibly shows a spread and an anticorrelation with Na.

ACKNOWLEDGEMENTS

SV and CMB acknowledge the support provided by Fondecyt Regular 1130721 and 1150060, respectively. PA acknowledges the support provided by the Chinese Academy of Sciences President's International Fellowship Initiative, Grant no. 2014FFJB0018, and by the Programa de Astronomia, Fondo China-Conicyt 2Conv. CAS15020.

REFERENCES

Alonso A., Arribas S., Martinez-Roger C., 1999, A&AS, 140, 261
Barklem P. S. et al., 2005, A&A, 439, 129
Bellazzini M., Ferraro F. R., Ibata R., 2003a, AJ, 125, 188
Bellazzini M., Ibata R., Ferraro F. R., Testa V., 2003b, A&A, 405, 577
Caloi V., D'Antona F., 2011, MNRAS, 417, 228
Carretta E. et al., 2009a, A&A, 505, 117
Carretta E. et al., 2009b, A&A, 505, 139
Carretta E. et al., 2010, A&A, 520, 95
Carretta E., Bragaglia A., Gratton R. G., D'Orazi V., Lucatello S., Sollima A., 2014, A&A, 561, 87
Cayrel R. et al., 2004, A&A, 416, 1117
Cristallo S., Straniero O., Piersanti L., Gobrecht D., 2015, ApJS, 219, 40
D'Ercole A., Vesperini E., D'Antona F., McMillan S. L. W., Recchi S., 2008, MNRAS, 391, 825
Francois P. et al., 2007, A&A, 476, 935
Fulbright J. P., 2000, AJ, 120, 1841
Gehren T., Shi J. R., Zhang H. W., Zhao G., Korn A. J., 2006, A&A, 451, 1065
Harris W. E., 1996, AJ, 112, 1487
Ibata R. A., Lewis G. F., 1998, ApJ, 500, 575
Ishigaki M. N., Aoki W., Arimoto N., Okamoto S., 2014, A&A, 562, 146
Ivans I. I., 2009, BAAS, 213, 341.06
Johnson J. A., Ivans I. I., Stetson P. B., 2006, ApJ, 640, 801
Kacharov N., Koch A., McWilliam A., 2013, A&A, 554, 81
Khalaj P., Baumgardt H., 2015, MNRAS, 452, 924
Koch A., McWilliam A., Grebel E. K., Zucker D. B., Belokurov V., 2008, ApJ, 688, 13
Kurucz R. L., 1970, SAO Special Report, 309
Law D. R., Majewski S. R., 2010, ApJ, 718, 1128
Marino A. F., Villanova S., Piotto G., Milone A. P., Momany Y., Bedin L. R., Medling A. M., 2008, A&A, 490, 625
Marino A. F., Milone A. P., Piotto G., Villanova S., Bedin L. R., Bellini A., Renzini A., 2009, A&A, 505, 1099
Monaco L., Bellazzini M., Bonifacio P., Ferraro F. R., Marconi G., Pancino E., Sbordone L., Zaggia S., 2005, A&A, 441, 141
Mottini M., Wallerstein G., McWilliam A., 2008, AJ, 136, 614
Mucciarelli A., Carretta E., Origlia L., Ferraro F. R., 2008, AJ, 136, 375
Mucciarelli A., Origlia L., Ferraro F. R., Pancino E., 2009, ApJ, 695, 134
Peterson R. C., Olszewski E. W., Aaronson M., 1986, ApJ, 307, 139
Pompeia L. et al., 2008, A&A, 480, 379
Pryor C., McClure R. D., Fletcher J. M., Hesser J. E., 1988, in Grindlay J. E., Philip A. G. D., eds, Proc. IAU Symp. 126, The Harlow-Shapley Symposium on Globular Cluster Systems in Galaxies. Kluwer, Dordrecht, p. 661
Ramirez I., Melendez J., 2005, ApJ, 626, 446
Reddy B. E., Tomkin J., Lambert D. L., Allende Prieto C., 2003, MNRAS, 340, 304
Reddy B. E., Lambert D. L., Allende Prieto C., 2006, MNRAS, 367, 1329
Sbordone L., Bonifacio P., Buonanno R., Marconi G., Monaco L., Zaggia S., 2007, A&A, 465, 815
Sbordone L. et al., 2015, A&A, 579, 104
Shetrone M. D., Cote P., Sargent W. L. W., 2001, ApJ, 548, 592
Simmerer J., 2004, BAAS, 205, 7705
Sneden C., 1973, ApJ, 184, 839
Stetson P. B., Catelan M., Smith H. A., 2005, PASP, 117, 1325
Ventura P., D'Antona F., 2009, A&A, 499, 835
Villanova S., Geisler D., 2011, A&A, 535, 31
Villanova S., Geisler D., Piotto G., 2010, ApJ, 722, 18
Villanova S., Geisler D., Carraro G., Moni Bidin C., Muñoz C., 2013, ApJ, 778, 186
Worley C. C., Hill V., Sobeck J., Carretta E., 2013, A&A, 553, 47

This paper has been typeset from a TEX/LATEX file prepared by the author.